*Cerebral Cortex*, January 2017;27: 474–484

**doi:10.1093/cercor/bhv240**
Advance Access Publication Date: 22 October 2015
Original Article



ORIGINAL ARTICLE

# The Effects of the X Chromosome on Intrinsic Functional Connectivity in the Human Brain: Evidence from Turner Syndrome Patients

Sheng Xie[1,†], Jiaotian Yang[3,†], Zhixin Zhang[2,†], Chenxi Zhao[3], Yanchao Bi[3], Qiuling Zhao[2], Hui Pan[4] and Gaolang Gong[3]

[1]Department of Radiology, [2]Department of Pediatrics, China-Japan Friendship Hospital, Beijing 100029, China, [3]State Key Laboratory of Cognitive Neuroscience and Learning & IDG/McGovern Institute for Brain Research, Beijing Normal University, Beijing 100875, China and [4]Key Laboratory of Endocrinology, Ministry of Health, Department of Endocrinology, Peking Union Medical College Hospital, Chinese Academy of Medical Sciences, Beijing 100730, China

Address correspondence to Gaolang Gong, PhD, State Key Laboratory of Cognitive Neuroscience and Learning, Beijing Normal University, Beijing 100875, China. Email: gaolang.gong@bnu.edu.cn

[†]These authors contributed equally to this work.

## Abstract

Turner syndrome (TS), a disorder caused by the congenital absence of one of the 2 X chromosomes in female humans, provides a valuable human "knockout model" for studying the functions of the X chromosome. At present, it remains unknown whether and how the loss of the X chromosome influences intrinsic functional connectivity (FC), a fundamental phenotype of the human brain. To address this, we performed resting-state functional magnetic resonance imaging and specific cognitive assessments on 22 TS patients and 17 age-matched control girls. A novel data-driven approach was applied to identify the disrupted patterns of intrinsic FC in TS. The TS girls exhibited significantly reduced whole-brain FC strength within the bilateral postcentral gyrus/intraparietal sulcus, angular gyrus, and cuneus and the right cerebellum. Furthermore, a specific functional subnetwork was identified in which the intrinsic FC between nodes was mostly reduced in TS patients. Particularly, this subnetwork is composed of 3 functional modules, and the disruption of intrinsic FC within one of these modules was associated with the deficits of TS patients in math-related cognition. Taken together, these findings provide novel insight into how the X chromosome affects the human brain and cognition, and emphasize an important role of X-linked genes in intrinsic neural coupling.

**Key words:** functional module, intrinsic functional connectivity, resting state functional MRI, the X chromosome, Turner syndrome

## Introduction

In addition to sex determination, the X chromosome is believed to play a crucial role in the development of the human brain and intelligence (Lehrke 1972; Turner 1996; Johnson et al. 2009). X-linked gene defects have been disproportionately observed in various neuropsychiatric disorders, particularly mental retardation (Ropers and Hamel 2005; Skuse 2005). Empirically ascertaining the patterns in which the X chromosome influences human brain structure and function is of particular importance for understanding sex differences in the brain and cognition

and for elucidating sex-specific incidences and symptom presentations for the majority of neuropsychiatric disorders.

In recent years, intrinsic functional connectivity (FC), a measure derived from resting-state functional magnetic resonance imaging (rs-fMRI), has emerged as an effective tool for exploring large-scale human brain organization (Biswal et al. 1995; Buckner et al. 2013). Using this powerful tool, landmark observations such as the default mode network (DMN) have been revealed (Greicius et al. 2003; Raichle 2010). Developmental processes and brain diseases can alter the patterns of intrinsic FC (Greicius 2008; Di Martino et al. 2014). Moreover, intrinsic FC is strongly associated with individual differences in cognitive performance, suggesting a critical role of intrinsic FC in cognition (Hampson et al. 2006; Baldassarre et al. 2012; Wei, Liang, et al. 2012). However, it remains unknown whether and how the X chromosome affects the intrinsic FC of the human brain, and this understanding may provide critical insight into the neural mechanisms underlying X-linked cognitive profiles in health or disease.

Turner syndrome (TS), a disorder in female humans that is characterized by the absence of a normal second X chromosome, serves as a unique human "knockout model" to study X chromosome function in the nervous system (Sybert and McCauley 2004). In TS patients, specific cognitive deficits, such as inferior visuospatial, math, and social cognitive abilities, caused by the loss of the X chromosome have been well documented (Rovet 2004; Hong and Reiss 2012). Neuroanatomically, TS patients have been shown to have reduced parieto-occipital gray matter (GM) volume (Murphy et al. 1993; Reiss et al. 1995; Molko et al. 2004; Marzelli et al. 2011), aberrant thickness and/or surface area of temporal-parieto-occipital cortical regions (Raznahan et al. 2010; Lepage, Clouchoux, et al. 2013; Lepage, Hong, et al. 2013; Lepage, Mazaika, et al. 2013), and impaired microstructural integrity of white matter (WM) tracts such as the superior longitudinal fasciculus (Holzapfel et al. 2006; Yamagata et al. 2012). Furthermore, functional MRI studies have revealed that during visuospatial (Kesler et al. 2004; Bray et al. 2013), executive function (Tamm et al. 2003), working memory (Haberecht et al. 2001; Hart et al. 2006; Bray et al. 2011), or arithmetic tasks (Molko et al. 2003; Kesler et al. 2006), TS patients show abnormal profiles of functional activation or functional coupling/connectivity, predominantly in the frontal/parietal cortices and in subcortical regions such as the caudate. However, currently, the patterns of intrinsic FC in TS patients remain unexplored.

Given the previously observed abnormalities in brain structure and function, we hypothesized that the loss of the X chromosome would result in severe disruption of intrinsic FC patterns in TS, likely affecting a specific functional circuit/network that accounts for the particular cognitive deficits of TS patients. To test this hypothesis, we performed rs-fMRI and obtained a set of cognitive assessments from female TS patients and controls. Using a novel data-driven approach, intrinsic FC was comprehensively analyzed to characterize the disrupted patterns of FC in TS.

## Methods and Materials

### Participants

Twenty-two TS girls with a nonmosaic 45XO karyotype (age range: 9–18 years) were recruited from the China-Japan Friendship Hospital (CJFH) and Peking Union Medical College Hospital (PUMCH). Age-matched healthy controls (HCs) (21 girls; age range: 10–18 years) were recruited from the local community and parent networks. For each TS patient, the nonmosaic 45XO karyotype was confirmed using a standard cytogenetic assessment of peripheral blood. All of the patients showed defective ovarian development, which was verified via pelvic ultrasound tests. Among the TS patients, 20 were on growth hormone (GH) treatment or had a history of such treatment, and only 4 were on estrogen replacement (ER) therapy. The medical history of all of the participants was screened to ensure that there was no evidence of current or past major neurological or psychiatric disorders. Additionally, no visible abnormalities (e.g., WM hypointensity) were observed on the MRI scans, which were examined by an experienced radiologist. For each participant, the travel and accommodation expenses for participating in this study were reimbursed. The research protocol was approved by the Research Ethics Committee of Beijing Normal University. For each participant, informed written consent was obtained from her legal guardian.

### Cognitive Assessment

For each participant, the cognitive assessments were performed within 2 days before or after the MRI scan. The participants aged 6–16 years were assessed using the Chinese version of the Wechsler Intelligence Scale for Children, Fourth Edition (WISC-IV), and 5 composite scores were generated: the full-scale intelligence quotient (FSIQ), verbal comprehension index (VCI), perceptual reasoning index (PRI), processing speed index (PSI), and working-memory index (WMI). Given that math-related cognitive deficiency has been consistently reported in TS, we further assessed all of the participants using 3 math tasks—simple subtraction, number comparison, and numerosity comparison (Wei, Lu et al. 2012)—online through a web-based program (http://www.dweipsy.com/lattice/). For the simple subtraction test, the cognitive score was computed by subtracting the number of incorrect responses from the number of correct responses per minute. For the number and numerosity comparison tests, the average reaction time of the correct trials divided by the accuracy was calculated, and the inverse of that result was used as the cognitive score, such that higher scores corresponded to better performance. The cognitive scores of the 3 tasks were significantly correlated across all participants (simple subtraction vs. number comparison, $R = 0.72$, $P < 0.01$; simple subtraction vs. numerosity comparison, $R = 0.33$, $P = 0.04$; and number comparison vs. numerosity comparison, $R = 0.46$, $P < 0.01$). For simplicity, we obtained a composite score to represent each participant's overall math ability by averaging the Z-scores of the 3 tasks for each participant. The individual Z-score for each task was computed using the mean and standard deviation (SD) of the HC group. This Z-score was highly correlated with Z-score obtained by using the mean and SD of the entire sample ($R = 0.998$).

### MRI Acquisition

All MRI scans were performed using the same 3 T Siemens Tim Trio MRI scanner in the Imaging Center for Brain Research, Beijing Normal University. For each participant, the head was fixed using straps and foam pads to minimize head movement.

#### *rs-fMRI*

During the scan, the participants were instructed to relax and be still with their eyes closed while remaining awake and not thinking systematically. According to a questionnaire after the scan, none of the participants fell asleep. The data were axially acquired using the following echo-planar imaging sequence: 33 axial slices; repetition time (TR), 2000 ms; echo time (TE), 30 ms; flip angle, 90°; slice thickness/gap, 3.5/0.7 mm; acquisition

matrix, 64 × 64; 3.1 × 3.1 mm in-plane resolution; and 200 volumes in total.

#### *High-resolution $T_1$-weighted Image*

High-resolution 3D $T_1$-weighted images were sagittally acquired by using a magnetization prepared rapid gradient echo (MPRAGE) sequence: 144 slices; TE, 3.39 ms; TR, 2530 ms; inversion time (TI), 1100 ms; 1.33 mm slice thickness with no gap; acquisition matrix, 256 × 256; and 1 × 1 mm in-plane resolution.

### rs-fMRI Preprocessing

rs-fMRI preprocessing was performed using the pipeline tool Data Processing Assistant for Resting-State fMRI (DPARSF) (Yan and Zang 2010). Briefly, the first 10 volumes were removed due to $T_1$ equilibration effects and the participants' adaption to the scanner. The remaining volumes were then corrected for slice time differences due to interleaved acquisition, realigned to the first volume to correct for head motion, and normalized to Montreal Neurological Institute (MNI) space. To improve the normalization accuracy, we used a pediatric $T_1$ template (http://www.bic.mni.mcgill.ca/ServicesAtlases). The age range of this template is 13.0–18.5 years (Fonov et al. 2011), which fits well with the age range of our participants. Specifically, for each participant, the rs-fMRI scan was first coregistered with the native $T_1$ image that was subsequently normalized to the pediatric template. The rs-fMRI scans were accordingly transformed into the MNI space, such that the image was resampled into 3 mm isotropic voxels. This procedure was implemented in SPM8 (http://www.fil.ion.ucl.ac.uk/spm, Friston et al. 1994). Next, the normalized rs-fMRI scans were spatially smoothed with a 6 mm full-width at half-maximum Gaussian kernel, linearly detrended, and temporally band-pass filtered (0.01–0.08 Hz). As generally recommended, 9 common nuisance variables were regressed out, including 6 head motion parameters (3 translations and 3 rotations along the *x*, *y*, and *z* axes), the global mean signal, the WM signal and the cerebrospinal fluid signal (Fox et al. 2005).

Notably, the data from 2 HCs were excluded because their head motion exceeded 2 mm or 2° in a specific direction. In addition, recent rs-fMRI studies regarding head motion have suggested that mean frame-wise displacement (FD) can be used to effectively estimate micromovement (Power et al. 2012). Individuals with a mean FD of more than 2 SDs from the mean of all of the participants should be excluded (Di Martino et al. 2013). We applied this exclusion criterion in the present study. Accordingly, the imaging data from one HC were discarded. Finally, the rs-fMRI data for 22 TS patients (mean age: 14.2 years; SD: 2.7 years) and 17 HCs (mean age: 14.1 years; SD: 2.3 years) were used for subsequent analysis. Moreover, we used the FD to determine the micromovements of the brain volumes during rs-fMRI scanning. Specifically, volumes with an FD >0.5 mm, along with the immediately preceding volume and 2 subsequent volumes, were considered micromovement-containing volumes (Power et al. 2012; Abrams et al. 2013).

### Whole-Brain FC Strength

First, we measured whole-brain functional connectivity strength (wFCS). A GM mask was generated by applying a threshold of 0.1 to the GM probability map of the pediatric template. Then, Pearson correlations of the blood oxygen level-dependent (BOLD) series between every pair of voxels within the GM mask were calculated and converted to Fisher's *Z*-values, which represent the strength of voxel pair-wise FC in the resting state. For a given voxel, its *Z*-values with every other voxel were summed together, which was defined as the wFCS value of that voxel (Buckner et al. 2009; Tomasi and Volkow 2010; Wang et al. 2014). Notably, because removing the global BOLD signal during preprocessing can introduce ambiguous negative functional correlations, only positive correlations (i.e., Z-value > 0) were counted for the wFCS, as described previously (Buckner et al. 2009; Liang et al. 2013).

The wFCS values for each voxel were statistically compared between the TS and HC groups, using 2-sample *t*-tests (two-tailed). Age was included as a covariate. To correct for multiple comparisons, the Monte Carlo simulation method was applied using the "3dClustSim" function of the AFNI package (Cox 1996). Family-wise error (FWE) corrected *P* values that were <0.05 at the cluster level were considered significant. To evaluate the influence of weak positive correlations (i.e., potential noise) on the results, we further compared the 2 groups using 2 other wFCS maps. Specifically, the 2 additional wFCS maps were calculated after eliminating weak positive correlations, that is, thresholding the voxel pair-wise correlation at 0.1 and 0.2 ($R > 0.1$ and $R > 0.2$), respectively.

### Identifying Relevant Subnetwork and Functional Modules

For brain clusters showing a significant wFCS group difference, the TS-associated FC alterations were indicated in a whole-brain manner. To further identify specific functional circuits/subnetworks, additional seed-based FC analyses were conducted. Specifically, each of the clusters identified above (6 in total) was taken as a seed. For each seed cluster, the representative BOLD series was extracted as the mean series from a sphere with a radius of 6 mm that was centered on the statistically determined peak voxel (Fox et al. 2005). Pearson correlations of the BOLD series between the seed and every other voxel within the GM mask were computed and converted into *Z*-values. For each seed cluster, a *Z*-map of FCS was generated for each subject.

Similarly, a 2-sample *t*-test that also considered age as a covariate was applied to detect intergroup differences in the *Z*-map for each seed region. Because only positive correlations were considered in the present study, the group comparison was constrained by a mask based on the voxels that showed a positive mean FC (i.e., Z-value > 0) in the HC group. To correct for multiple comparisons, the method of Monte Carlo simulation was performed using "3dClustSim".

A set of clusters (referred to as target clusters) showed significantly reduced FCS with the seed clusters in the TS patients compared with the HCs. The intrinsic FC of all of these target and seed clusters was putatively affected by the loss of the X chromosome in the TS patients. We therefore selected these clusters to establish a functional subnetwork in which each seed or target cluster represented a node (a total of 31 nodes). A similar approach was applied in a recent study (Gotts et al. 2012). Again, the representative BOLD series for each node/cluster was extracted by averaging the series within a sphere with a radius of 6 mm that was centered on the calculated peak voxel. For each subject, we generated a node-by-node correlation matrix (also converted to a *Z*-matrix) that represented the functional subnetwork. Within each group, a one-sample *t*-test (one-tailed) was first applied to all of the node pairs (595 in total) to determine whether the converted *Z*-value was significantly greater than zero (i.e., significantly positive at the group level). Here, the false discovery rate (FDR) approach was used to correct for multiple comparisons, and $q < 0.05$ was considered significant. For the between-node

connections that were significantly positive at the group level in either the HC or TS group, we performed a 2-sample *t*-test to evaluate intergroup differences, and the FDR method was applied to correct for multiple comparisons.

For each group, the average functional subnetwork (i.e., the average Z-matrix) across individuals was obtained, and the Z-values of the node pairs that showed non-significantly positive correlations at the group level were removed (i.e., set to zero). A modular analysis was then performed on the average Z-matrix to explore whether this functional subnetwork could be subdivided into different functional modules. Specifically, a spectral reordering algorithm was applied (Newman 2006).

### Correlating Intrinsic FC Changes to Math Ability Deficits in TS

To evaluate whether the observed FC abnormalities could account for the math ability deficits of TS girls, we examined the correlations between the composite math score and the FC parameters across subjects in both the TS and HC groups, adjusting for age. The FC parameters included the voxel-wise wFCS across the entire GM, the wFCS of the identified clusters, the FCS of the connections in the identified subnetwork, and the mean FCS of the identified functional modules.

## Results

### Demographics and Cognitive Assessment

The demographic information and the results of the cognitive assessment are summarized in Table 1. No significant difference in age was observed between the groups ($P = 0.87$). The TS patients had significantly lower values for the 5 IQ scores: FSIQ ($P = 0.0004$), WMI ($P = 0.03$), VCI ($P = 0.01$), PRI ($P = 0.0004$), and PSI ($P = 0.0004$). The TS patients also scored lower than the HCs on the 3 math tasks (simple subtraction: $P = 0.03$; number comparison: $P = 0.007$; and numerosity comparison: $P = 0.02$) as well as on overall math ability (composite score: $P = 0.003$).

### wFCS Differences

First, several head motion parameters were compared between the TS and HC groups, but no significant difference was observed (maximum head displacement, $P = 0.51$; maximum head rotation, $P = 0.54$; mean FD, $P = 0.80$). Moreover, the number of rs-fMRI brain volumes with micromovement also did not differ significantly between the 2 groups (HC: 9.4 ± 13.5, range 0–40; TS: 5.4 ± 7.2, range 0–27; $P = 0.24$).

On the GM mask, the total wFCS was significantly smaller in the TS group than in the HC group (HC: $0.36 \pm 0.03 \times 10^9$; TS: $0.34 \pm 0.02 \times 10^9$; $P = 0.02$). The mean wFCS maps for both groups are illustrated at the voxel level in Figure 1. The 2 maps exhibited very similar spatial patterns of voxel-wise wFCS; the highest wFCS values occurred within several DMN regions, including the posterior cingulate gyrus (PCC)/precuneus, the medial prefrontal cortex (MPFC) and the inferior parietal lobule (IPL). The insula and the postcentral gyrus (PoCG) also showed relatively high wFCS values. The observed spatial distribution of wFCS was highly consistent with that reported in previous studies (Tomasi and Volkow 2010; Wang et al. 2014).

Visual inspection indicated reduced wFCS values for the TS group in multiple brain regions. The statistical comparison revealed 6 clusters that exhibited significantly reduced wFCS in the TS group compared with the HC group (FWE-corrected $P < 0.05$, Fig. 1). These 6 clusters were located in (1) the cuneus, (2) the right cerebellum, (3) the right PoCG/intraparietal sulcus (IPS), (4) the left PoCG/IPS, (5) the right angular gyrus (ANG), and (6) the left ANG. The details are summarized in Table 2. The statistical map was closely replicated when the wFCS that eliminated weak correlations was used (Supplementary Figure 1), suggesting that the wFCS thresholding value had a limited effect on our results. Moreover, to evaluate the effect of head micromovements on this result, we removed the micromovement rs-fMRI volumes from the entire time series for each individual and reran the analysis. Statistically, the results remained almost the same (data not shown), indicating a limited effect of head micromovement on our results.

### Relevant Subnetworks and Modules

By considering each significant wFCS cluster as a seed, we next performed seed-based FC analysis. For each of the seeds, a set of clusters (referred to as a target cluster) was observed, and the FCS between the seed and the target cluster was significantly reduced in the TS group compared with the HC group (i.e., FWE-corrected $P < 0.05$). In total, we observed 26 significant target clusters for the 6 seed clusters. We did not find any significant target clusters with increased FCS in the TS patients. The identified target

**Table 1** Demographic characteristics and cognitive assessment performance

| | HC ($n = 17$) | TS ($n = 22$) | Intergroup comparison (*P* value) |
|---|---|---|---|
| Age (years) | 14.1 ± 2.3 | 14.2 ± 2.7 | 0.87 |
| Intelligence quotient (IQ) | | | |
| FSIQ | 108.4 ± 12.7 (16) | 88.3 ± 16.1 (17) | 0.0004 |
| WMI | 100.3 ± 15.5 (16) | 88.2 ± 15.6 (17) | 0.03 |
| VCI | 117.1 ± 11.6 (16) | 101.8 ± 20.5 (17) | 0.01 |
| PRI | 102.2 ± 12.6 (16) | 83.5 ± 14.1 (17) | 0.0004 |
| PSI | 104.1 ± 16.9 (16) | 84.2 ± 11.6 (17) | 0.0004 |
| Math-related task | | | |
| Simple subtraction | 43.44 ± 8.33 (16) | 35.24 ± 12.05 (21) | 0.03 |
| Number comparison | 0.0016 ± 0.00032 (16) | 0.0013 ± 0.00031 (21) | 0.007 |
| Numerosity comparison | 0.0012 ± 0.00026 (16) | 0.0010 ± 0.00025 (21) | 0.02 |
| Composite Z-score | 0 ± 0.73 (16) | −0.86 ± 0.91 (21) | 0.003 |

Note: The bracket after the cognitive scores represents the number of subjects who successfully performed the cognitive test. HC, healthy control; TS, Turner syndrome; FSIQ, full-scale intelligence quotient; WMI, working memory index; VCI, verbal comprehension index; PRI, perceptual reasoning index; PSI, processing speed index.

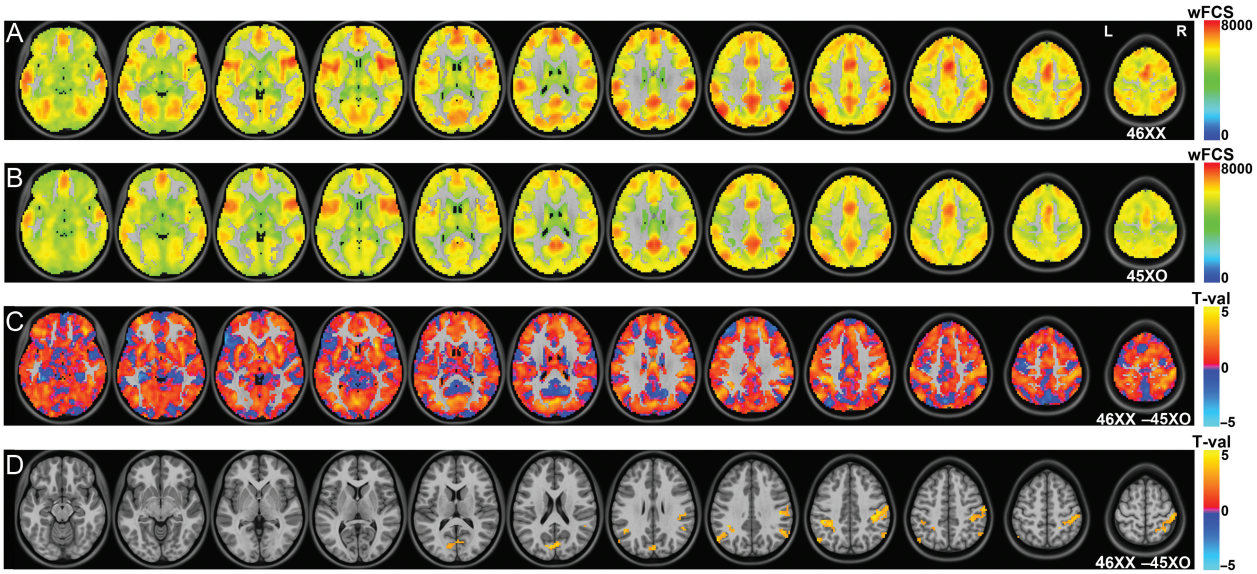


**Figure 1.** The wFCS differences between the HC and TS groups. Here, 46XX and 45XO represent the karyotypes of HC and TS girls, respectively. (*A*) The mean wFCS map for the HC group. (*B*) The mean wFCS map for the TS group. (*C*) The T map for the differences between the HC and TS groups. (*D*) The clusters showing significantly reduced wFCS values in TS patients compared with the HCs (FWE-corrected $P < 0.05$). HC, healthy control; TS, Turner syndrome.

clusters were primarily observed within the superior parietal lobule (SPL)/IPL and surrounding areas, the PCC/precuneus, the MPFC/lateral prefrontal cortex (LPFC), the middle/inferior temporal cortex (MTC/ITC), the pericalcarine visual cortex, and the cerebellum (Fig. 2 and Table 2). Overall, the identified target clusters exhibited a bilaterally symmetrical pattern despite a few unilaterally distributed target clusters. The 2 seed clusters in the left and right ANG exhibited a very similar spatial distribution of target clusters. Notably, some target clusters from one seed cluster spatially overlapped with other seed clusters or with target clusters from another seed cluster, indicating circuit-like relationships between these clusters (Fig. 2 and Table 2).

Taken together, we identified 31 separate nodes (6 seed clusters and 25 target clusters). The seed cluster in the left PoCG/IPS highly overlapped with the target cluster from the seed cluster in the right PoCG/IPS (and mapped to identical MNI coordinates); therefore, they were counted as a single node. For each individual, a 31 × 31 Pearson correlation matrix was generated. The average Z-matrices for both groups are illustrated in Figure 3.

Furthermore, the spectral reordering algorithm revealed 3 modules for the average Z-matrix in the HC group. Within each module, the nodes were densely connected. However, very few connections were detected between modules. Notably, the modular organization was apparent only in the reordered matrices, as illustrated in Figure 3. To simplify interpretation, the average Z-matrix for the TS group was reordered in terms of the modules that were identified in the HC group.

Specifically, Module I was composed of 3 vision-related nodes (i.e., the seed cluster in the cuneus and 2 related target clusters). Module II contained 12 nodes, including 3 seed clusters (the right cerebellum and the left and right PoCG/IPS) and their related target clusters. The remaining 16 nodes formed Module III, which consisted of 2 seed clusters (i.e., the left and right ANG) and their related target clusters. These details are presented in Table 2.

As illustrated in Figure 3, the TS group visually showed less or weaker FC in each of the 3 modules. Given the node selection criteria described above, the reduction of FC between the seed cluster and its corresponding target clusters was expected, but it remains unknown whether there are FCS differences in the connections between different seed or target clusters. The results presented here also revealed significant reductions in FC between many different seed or target clusters. The reduced FCS values were evenly distributed across the 3 modules, without showing a preference for any specific module. Notably, a few increases in FC between modules were observed.

### Functional Module Disruption versus Math Ability Deficits in TS

The voxel-wise correlation between the wFCS and composite math score across the entire GM showed no significant cluster after multiple comparison correction (i.e., FWE-corrected $P > 0.05$). The wFCS values of the 6 wFCS clusters were not significantly correlated with the composite math score ($P > 0.05$), but the cluster in the right ANG displayed a trend toward such a correlation ($R = 0.29$, $P = 0.08$). In addition, none of the connections within the subnetwork remained significant ($P < 0.05$) after FDR correction for the correlation between FCS and the math scores.

Considering each module as a whole, the modular mean FCS was significantly correlated with the math score for Module II ($R = 0.43$, $P = 0.009$) but not Module I ($R = 0.21$, $P = 0.23$) or III ($R = 0.20$, $P = 0.23$). The scatter plot for Module II is shown in Figure 4. To assess whether Module II was at least partially specific for math-related cognitive processing, we further examined whether the mean FCS of Module II correlated with the VCI score. A trend toward a positive correlation was observed ($R = 0.32$, $P = 0.07$). Crucially, however, the correlation of the mean FCS of Module II with the math score remained marginally significant ($R = 0.35$, $P = 0.056$) after controlling for the VCI score, indicating that the contribution of Module II to math processing could not be fully attributed to the effects of general cognitive ability.

## Discussion

Using a cohort of TS patients and HCs, the present study comprehensively investigated how the X chromosome affects intrinsic

**Table 2** Clusters/ROIs showing differences in resting-state functional connectivity in TS girls

| | Cluster/ROIs | MNI coordinates of the cluster peak | | | Volume ($mm^3$) | Modular index |
|---|---|---|---|---|---|---|
| | | X | Y | Z | | |
| **1** | **Cuneus** | **−6** | **−78** | **18** | **2403** | **1** |
| 2 | Pericalcarine occipital cortex | −27 | −63 | −18 | 26 568 | 1 |
| 3 | Superior/middle occipital cortex | 27 | −78 | 18 | 2916 | 1 |
| **4** | **Right cerebellum** | **21** | **−72** | **−54** | **3132** | **2** |
| 5 | Left supramarginal gyrus | −63 | −36 | 39 | 4239 | 2 |
| 6 | Right anterior fusiform gyrus | 27 | −6 | −39 | 3105 | 2 |
| 7 | Left anterior fusiform gyrus/inferior temporal gyrus | −33 | −6 | −42 | 2565 | 2 |
| **8** | **Right postcentral gyrus/Intraparietal sulcus** | **39** | **−30** | **42** | **12 123** | **2** |
| 9 | Left postcentral gyrus/Intraparietal sulcus | −45 | −36 | 39 | 11 151 | 2 |
| **9** | **Left postcentral gyrus/Intraparietal sulcus** | **−45** | **−36** | **39** | **2538** | **2** |
| 10 | Right postcentral gyrus/intraparietal sulcus | 30 | −39 | 48 | 15 093 | 2 |
| 11 | Right posterior superior/middle frontal gyrus | 30 | 0 | 66 | 8613 | 2 |
| 12 | Right SPL | 27 | −57 | 69 | 6831 | 2 |
| 13 | Right posterior inferior frontal gyrus | 51 | 15 | 33 | 6183 | 2 |
| 14 | Left posterior superior/middle frontal gyrus | −27 | 0 | 48 | 4158 | 2 |
| 15 | Left anterior supramarginal gyrus | −63 | −27 | 39 | 4023 | 2 |
| **16** | **Right angular gyrus** | **51** | **−54** | **33** | **1998** | **3** |
| 17 | Medial/LPFC | −33 | 66 | 0 | 57 537 | 3 |
| 18 | Left middle/inferior temporal gyrus | −63 | −21 | 15 | 17 955 | 3 |
| 19 | Right cerebellum-crus | 18 | −90 | −27 | 12 096 | 3 |
| 20 | Precuneus/PCC | 9 | −42 | 36 | 10 125 | 3 |
| 21 | Left angular gyrus/intraparietal sulcus | −45 | −66 | 57 | 9018 | 3 |
| 22 | Right middle/inferior temporal gyrus | 72 | −30 | −9 | 8532 | 3 |
| 23 | Right ventrolateral prefrontal cortex | 39 | 54 | −15 | 6507 | 3 |
| **24** | **Left angular gyrus** | **−45** | **−57** | **33** | **2592** | **3** |
| 25 | Medial/lateral prefrontal cortex | 6 | 51 | 21 | 38 853 | 3 |
| 26 | Left middle temporal gyrus | −54 | 15 | −33 | 13 554 | 3 |
| 27 | Posterior cingulate gyrus/precuneus | −3 | −30 | 42 | 10 179 | 3 |
| 28 | Right temporal pole | 45 | 21 | −30 | 6804 | 3 |
| 29 | Caudate | −12 | 9 | 12 | 4617 | 3 |
| 30 | Right angular gyrus | 54 | −51 | 27 | 4401 | 3 |
| 31 | Cerebellum-vermis | 6 | −57 | −42 | 3510 | 3 |

Note: The 6 seed clusters are marked in bold (i.e., the 1st, 4th, 8th, 9th, 16th, and 24th clusters), followed by their respective target clusters. Notably, the target cluster for the seed cluster of the right postcentral gyrus/intraparietal sulcus strongly overlapped with the seed cluster of the left postcentral gyrus/intraparietal sulcus (the ninth cluster); therefore, they were considered as a single node. The modular indexes 1, 2, and 3 correspond to Modules I, II, and III in Figure 3. MNI, Montreal Neurological Institute.

FC patterns in the human brain. Compared with the HCs, the TS patients had significantly decreased wFCS within the bilateral PoCG/IPS, ANG, and cuneus as well as the right cerebellum. Furthermore, a specific functional subnetwork was identified in which intrinsic FC between regions was typically reduced in the TS patients. This subnetwork could be divided into 3 functional modules, and the disruption of intrinsic FC within one of these modules was associated with the math-related cognitive deficits of the TS patients in. Together, these results elucidate the effect of the X chromosome on functional coupling in the human brain and provide important information to understand X-linked brain diseases and sex differences in the brain, specifically with respect to cognition.

The X chromosome, which comprises approximately 4% of the human genome, has long been considered to be critical for the development of the human brain and intelligence (Lehrke 1972; Turner 1996; Johnson et al. 2009). TS patients naturally lose one of their 2 normal X chromosomes; therefore, these individuals serve as a valuable human "knockout model" for studying how the X chromosome affects the human brain and cognition. A number of MRI studies have been conducted on TS patients, but they have primarily focused on structural brain anomalies or functional changes during specific cognitive tasks (Mullaney and Murphy 2009). The current investigation is the first study to explore the intrinsic FC patterns in TS, and our results may provide novel understanding to elucidate the function of the X chromosome in the nervous system. Further, the current study provides direct evidence of an X-linked genetic basis for intrinsic FC, which is of particular value for the identification of genes involved in this fundamental phenotype of the human brain.

It is important to note that X-linked genes can affect the brain in at least 2 ways: by directly acting on the brain and by indirectly acting on the gonads to induce differences in specific gonadal secretions (i.e., hormones) that exert specific effects on the brain (Arnold 2004). To isolate the direct genetic effect from the indirect hormonal effect, one possible approach is to ensure identical hormonal levels across individuals with different X-linked genotypes. Although identical hormone levels between adolescent TS patients and healthy controls are difficult to achieve in practice, a suboptimal alternative is to match the pubertal stage, as an approximation of the sex hormone level, between groups. In our cohort, however, pubertal status was not well matched between the

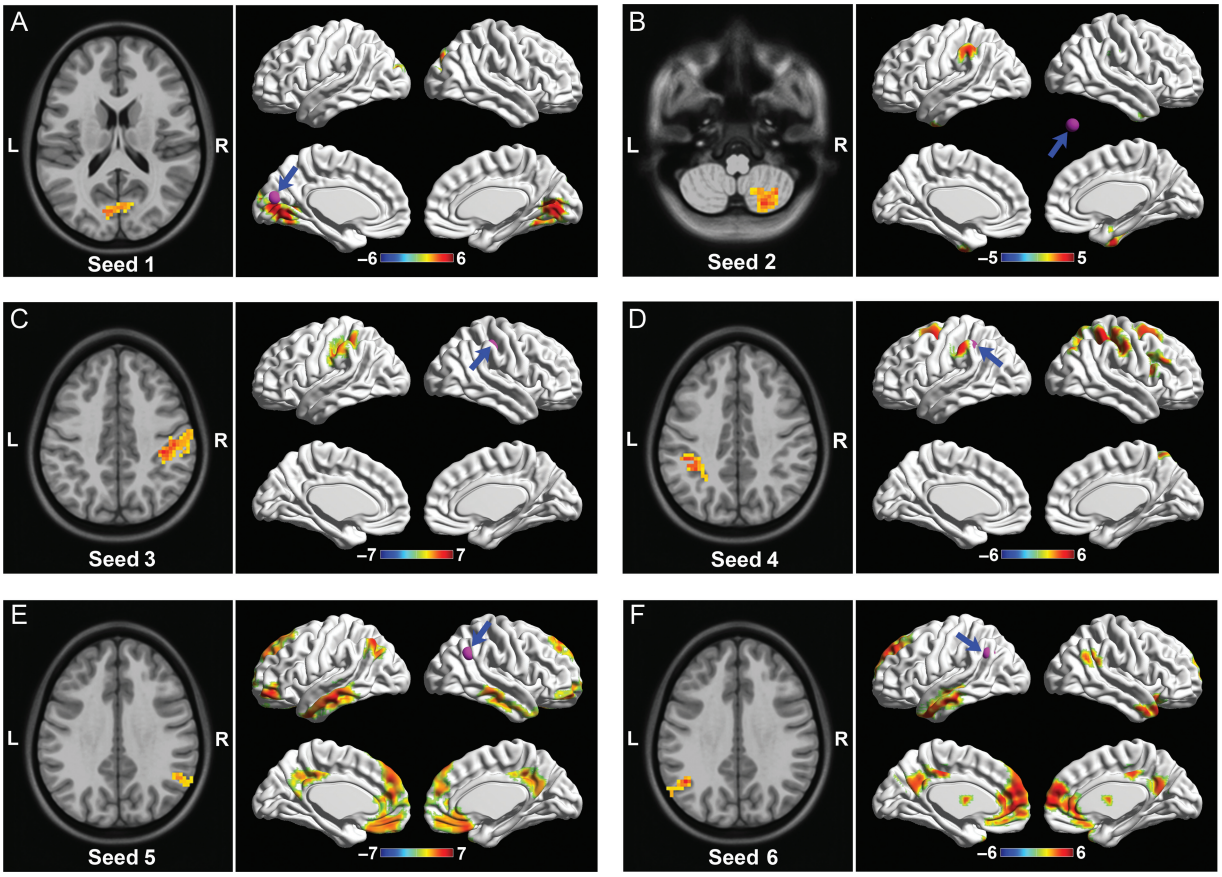


**Figure 2.** The target clusters showing a significant reduction in intrinsic FC with their seed clusters. (*A*) The target clusters for the seed region of the cuneus. (*B*) The target clusters for the seed region of the right cerebellum. (*C*) The target clusters for the seed region of the right PoCG/IPS. (*D*) The target clusters for the seed region of the left PoCG/IPS. (*E*) The target clusters for the seed region of the right ANG. (*F*) The target clusters for the seed region of the left ANG. The seed clusters were indicated by the purple balls and blue arrows. The colors indicate the T values for the intergroup differences. L, left; R, right.

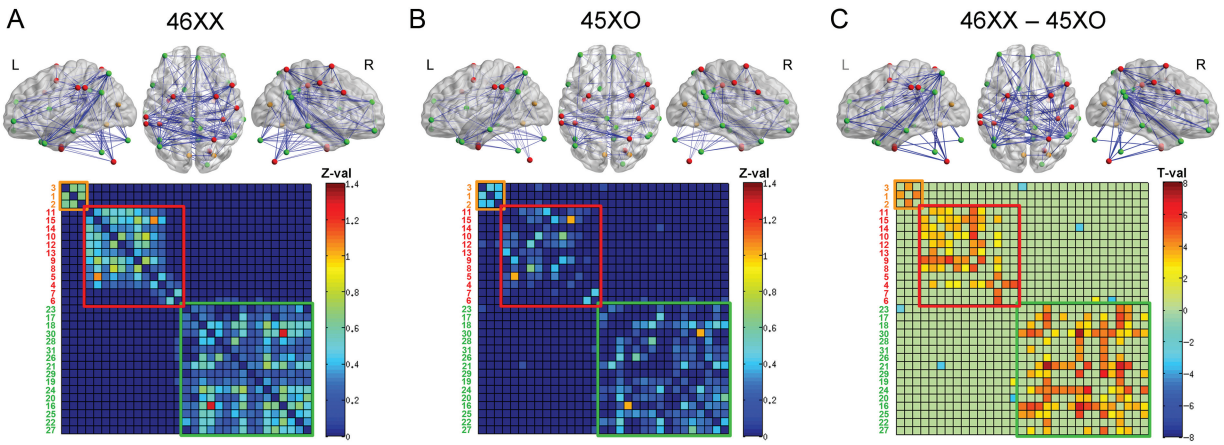


**Figure 3.** The relevant subnetwork and functional modules associated with the loss of the X chromosome in TS patients. 46XX and 45XO represent the karyotypes of HC and TS girls, respectively. (*A*) The relevant subnetwork and functional modules for the HC group. (*B*) The relevant subnetwork and functional modules for the TS group. In the 3D network rendering, the nodes within Modules I, II, and III are shown in yellow, red, and green, respectively. The colors in the matrix represent the mean Z values for the intrinsic FCS across the subjects. Modules I, II, and III are indicated by yellow, red and green rectangles, respectively, in the matrix. (*C*) The intergroup differences in intrinsic FC within the subnetwork and the modules. The colors in the matrix represent the *T*-values for the intergroup differences. The number for each row of the matrices correspond to the index of clusters/regions in Table 2. The 3D brain rendering was implemented using the Brainnet Viewer (Xia et al. 2013).

2 groups. The majority of our TS patients were prepubertal because spontaneous puberty is very rare in TS girls, and most of our TS patients did not undergo ER therapy to artificially induce puberty. Therefore, the intrinsic FC patterns observed in the TS patients may be due to a direct genetic factor, an indirect hormonal factor, or a combination of the 2. Future studies that employ animal models are essential to dissociate these 2 effects (Arnold and Chen 2009; Raznahan et al. 2013).

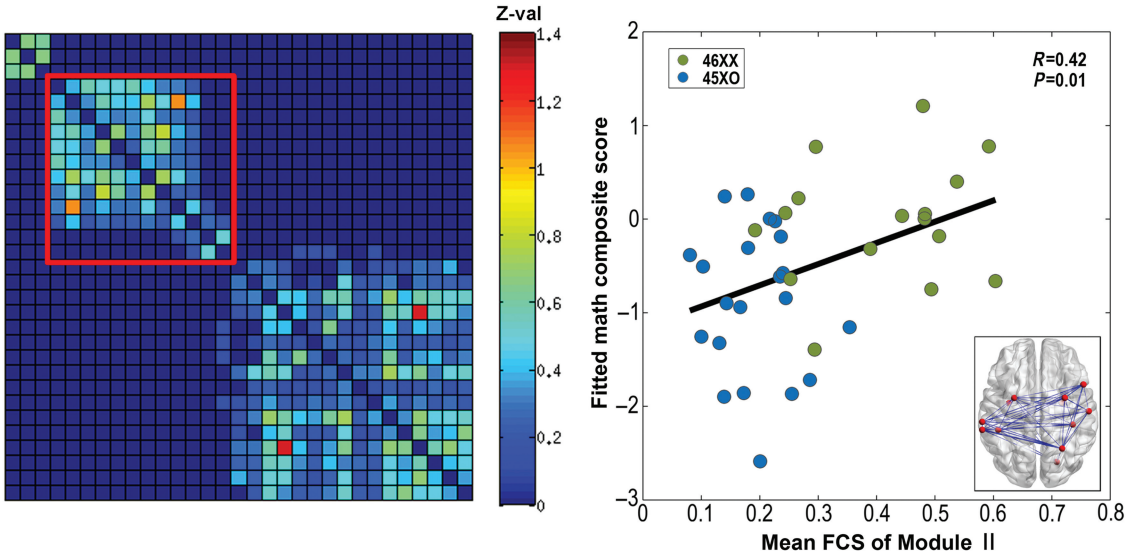


**Figure 4.** The correlation of math ability with the mean FCS of Module II in the subnetwork. Module II is indicated by a red rectangle in the matrix.

## Hub Regions of Disrupted Intrinsic FC

In the present study, intrinsic FC was measured by analyzing the correlations between BOLD signals in a resting state (Biswal et al. 1995; Buckner et al. 2013). To avoid a priori selection of specific regions of interest (ROIs), we used a data-driven approach to map the wFCS at the voxel level and identified the regions that showed aberrant FCS in the TS patients. Similar approaches have been applied to study mental dysfunction (Gotts et al. 2012; Wang et al. 2014) and to search for connectivity hubs within the brain (Buckner et al. 2009; Tomasi and Volkow 2010).

A set of regions including the bilateral IPS, ANG, cuneus, and cerebellum showed reduced wFCS in the TS patients compared with the HCs. Widespread FCS interruptions between these regions and other region across the entire brain are expected. Clearly, in terms of disrupted FC, these regions represent the most affected, or hub regions, and the FCS of these regions is strongly associated with the loss of the X chromosome. Consistently, these regions have been showed to exhibit structural abnormalities in TS. For instance, aberrant morphology, including abnormal sulcal geometry, cortical thickness, and GM volume, was observed for the IPS in TS females (Raznahan et al. 2010; Marzelli et al. 2011; Lepage, Clouchoux, et al. 2013; Molko et al. 2003). In addition, reduced cortical surface area and GM volume in the ANG and cuneus (Reiss et al. 1995; Marzelli et al. 2011; Xie et al. 2015), as well as increased GM volume in the cerebellum (Cutter et al. 2006; Hong, Hoeft, et al. 2014), have been found in TS. In line with these findings, the ANG and the cuneus also display sex differences in cortical thickness (Sowell et al. 2007), further supporting a function of the X chromosome in these regions.

Aside from the structural anomalies caused by the loss of the X chromosome, these hub regions display abnormal neuronal activity during the performance of cognitive tasks. During specific arithmetic tasks, the IPS, ANG and cuneus showed weaker functional activation in TS patients than in HCs (Molko et al. 2003; Kesler et al. 2006). Moreover, decreases in functional activation or BOLD signal changes were found within the IPS during working memory or visuospatial tasks (Haberecht et al. 2001; Kesler et al. 2004; Hart et al. 2006; Bray et al. 2011, 2013). In particular, during these tasks, abnormal FC seeding from the IPS has been observed (Bray et al. 2011, 2013). It is possible that for the IPS, the disrupted intrinsic FC in the resting state we observed serves as a baseline abnormality that contributes to the abnormal FC detected during various tasks.

The disrupted intrinsic FC of these regions observed in the TS patients should at least partially correlate with the structural and task-based functional abnormalities described above. However, the relationship between these factors might be very complex, and importantly, it is unclear whether these factors are causally associated with each other. Unraveling these relationships is critical for clarifying the functional pathway by which the X chromosome affects these regions. Future studies using multimodal imaging techniques would be useful for addressing this issue.

## Disrupted Functional Modules and Cognition

Based on the observed hub regions, we further identified a subnetwork in which the majority of the region/node pairs displayed reduced intrinsic FC in the TS patients compared with HCs. Importantly, this subnetwork is composed of 3 functional modules. Modular structure is a commonly observed feature of structural and functional brain networks (Chen et al. 2008; He et al. 2009). Such structure provides a balance between the 2 most fundamental principles of brain organization, functional segregation and integration, and facilitates efficient recurrent processing within modules and information exchange between modules (Sporns et al. 2000, 2004; Kotter and Stephan 2003). Within each module, a set of regions/nodes is densely connected, putatively allowing them to work together to perform certain functions. In TS patients, all 3 observed modules showed reduced intrinsic FC.

Intriguingly, the mean FCS of Module II was correlated with overall math ability, and therefore, the connectivity disruption of this module likely accounts for the math cognitive deficits of the TS patients relative to the controls. Notably, this significant correlation was based on the entire sample, and there was no significant correlation within either the TS ($R = -0.11$, $P = 0.64$) or the control group ($R = 0.21$, $P = 0.44$), suggesting that the FCS of Module II could not account for the within-group variance in math ability. The lack of significant within-group correlation might be due to the very small sample size, the narrow range, or the small variance of math scores within each group. The significant correlation across the entire sample suggests that the X chromosome might influence math cognition by modulating the

intrinsic FC of a math-specific functional module. Module II may serve as a backbone for such a math-specific functional module. Specifically, Module II consisted of 11 regions predominantly from the parietal cortex, including the IPS, the SPL and the supramarginal gyrus. These regions, particularly the IPS, have been well recognized to be involved in math-related cognitive processing (Molko et al. 2003; Wei et al. 2014), supporting the current results regarding Module II and math ability.

The other 2 modules were not correlated with the math cognitive scores, indicating the specificity of Module II for math cognition. The other 2 modules are likely associated with other cognitive functions. For instance, Module I included 3 visual regions that are located close together in the occipital cortex and that are highly involved in visuospatial cognition. Therefore, the disrupted connectivity of Module I may underlie the deficits of TS patients in visuospatial ability, another well-observed cognitive feature caused by loss of the X chromosome (Rovet 2004). In contrast, Module III consisted of 16 regions that are widely distributed across the brain; these regions are likely involved in multiple functional systems. For example, several regions, including the PCC/precuneus, the MPFC, and the ANG, are considered to be key nodes of the DMN (Fox et al. 2005). These DMN regions, together with other regions in Module III such as the middle/inferior temporal gyrus and the temporal poles, have been recognized as key nodes for social cognitive processing (Kennedy and Adolphs 2012). Accordingly, Module III may be associated with social cognition, and it is possible that the disruption of Module III is related to the social cognitive deficits of TS patients (Hong and Reiss 2012; Hong, Bray, et al. 2014). However, these interpretations of the cognitive functions of Modules I and III are essentially speculative. In the present study, the relevant cognitive tests were not performed on our participants and therefore this study did not provide the data needed to evaluate these speculations. This issue must be addressed in future studies.

To some extent, the reduced FC in our observed modules reflects a decreased efficiency of the underlying anatomical connectivity. This interpretation is supported by previous findings showing a reduction in WM integrity in TS patients (Molko et al. 2004; Holzapfel et al. 2006; Yamagata et al. 2012; Xie et al. 2015). However, some evidence clearly suggests that intrinsic FC is not simply a proxy for the underlying anatomical connectivity (Buckner et al. 2013). To elucidate the biological mechanisms underlying the intrinsic FC finding presented here, specific investigations at the molecular or cellar level are warranted.

Notably, the functional modules that were identified in the present study were extracted using a data-driven approach based on whole-brain FC. Due to our constraint of analyzing only the TS-affected FC, each of the functional modules might be incomplete. Alternatively, a set of ROIs based on previous fMRI studies of math, visuospatial, or social cognition could be applied as modular nodes, which would result relatively complete functional modules for these cognitive functions. However, the challenge of this type of approach is the selection of appropriate ROIs, particularly for cognitive functions such as math that are less studied and for which relatively mixed fMRI results have been obtained in humans.

### TS-related Math Deficits in Response Time or Accuracy

Previous studies have suggested that the math deficits in TS are mainly related to slower processing in math-related tasks rather than to overall accuracy (Bruandet et al. 2004; Mazzocco 2006). To evaluate whether the current math-related results were mainly attributed to response time or accuracy in the math-related tasks, we calculated separate composite scores for response time and accuracy. The 2 composite scores showed a significant difference or trend between the TS and control groups (t-test): composite response time, $P = 0.043$; composite accuracy, $P = 0.068$. This result suggests that both the response time and accuracy contributed to the group differences in overall math ability we observed (Table 1). To investigate the significant correlation observed between the mean FCS of Module II and the overall math composite score, we reran the correlational analysis with the response time and accuracy composite scores. While the 2 correlations were not significant (composite response time: $R = -0.28$, $P = 0.101$; composite accuracy: $R = 0.20$, $P = 0.237$), they were in the same direction as the correlation for the overall math composite score (i.e., the higher the FCS, the better the math ability; Fig. 4). Therefore, it is likely that the correlation we observed for the overall math composite score was related to both response time and accuracy.

It is important to note that these additional math-related analyses were explorative in nature and that the math-related tests in our study are not comprehensive. In addition, we did not apply a test to measure general/basic processing speed not specific to any particular tasks, and therefore we were not able to conduct math-related analyses in which the general processing speed had been corrected. Specific studies with more comprehensive math cognitive tests are desired to elucidate cognitive mechanisms underlying the math-related findings in TS patients reported here.

### Limitations and Future Work

Several methodological issues must be addressed. First, factors such as GH use, ER treatment, and X-linked imprinting may affect brain structures in TS patients (Cutter et al. 2006; Lepage, Clouchoux, et al. 2013; Lepage, Hong et al. 2013). In the present study, these factors could not be evaluated due to the limited sample size and the lack of related information. The effects of these potential confounding factors must be evaluated in the future. Second, the vast majority of our controls lives in urban area of Beijing city and experienced superior childhood socioeconomic status (e.g., parental education, occupation, and income). This background likely underlies the superior VCI scores of our control group. In contrast, the living environments of the TS girls were heterogeneous. The lack of living environment matching may confound our results to some extent, which should be evaluated in the future. Finally, given the very ambiguous biological meaning of negative FC (i.e., anti-correlations) in rs-fMRI, the present study excluded negative FC across the entire brain during the analysis, as done previously (Buckner et al. 2009; Liang et al. 2013). However, while negative FC is likely to be introduced artificially by removing the global BOLD signal during preprocessing, negative resting state FC under resting state does exist even without removing the global signal. Our current results therefore might be limited due to the exclusion of meaningful changes in negative FC in the TS patients.

## Conclusion

By showing reduced intrinsic FC in TS patients, the present study provides the first evidence for the effects of the X chromosome on this FC phenotype in the human brain. In particular, the observed intrinsic FC disruption was found to account for specific cognitive deficits caused by the loss of the X chromosome. These findings provide novel insight into how the X chromosome affects the human brain and cognition.

## Supplementary Material

Supplementary material can be found at: http://www.cercor.oxfordjournals.org/.

## Funding

This work was supported by the 863 program (2015AA020912), the 973 program (no.2013CB837300), the National Science Foundation of China (81271649, 81322021), the Beijing Nova Program (Z121110002512032), the Beijing Municipal Science & Technology Commission (no. Z151100003915117, Z151100003915122), the Specialized Research Fund for the Doctoral Program of Higher Education, China (no. 20130003110002), the GeneScience Scientific Research Funds, and the Fundamental Research Funds for the Central Universities.

## Notes

The authors thank Prof. Yong He for his valuable comments on the preprocessing of fMRI data. *Conflict of Interest*: None declared.

## References

Abrams DA, Lynch CJ, Cheng KM, Phillips J, Supekar K, Ryali S, Uddin LQ, Menon V. 2013. Underconnectivity between voice-selective cortex and reward circuitry in children with autism. Proc Natl Acad Sci USA. 110:12060–12065.

Arnold AP. 2004. Sex chromosomes and brain gender. Nat Rev Neurosci. 5:701–708.

Arnold AP, Chen X. 2009. What does the "four core genotypes" mouse model tell us about sex differences in the brain and other tissues? Front Neuroendocrinol. 30:1–9.

Baldassarre A, Lewis CM, Committeri G, Snyder AZ, Romani GL, Corbetta M. 2012. Individual variability in functional connectivity predicts performance of a perceptual task. Proc. Natl Acad. Sci. 109:3516–3521.

Biswal B, Yetkin FZ, Haughton VM, Hyde JS. 1995. Functional connectivity in the motor cortex of resting human brain using echo-planar MRI. Magn Reson Med. 34:537–541.

Bray S, Dunkin B, Hong DS, Reiss AL. 2011. Reduced functional connectivity during working memory in Turner syndrome. Cereb Cortex. 21:2471–2481.

Bray S, Hoeft F, Hong DS, Reiss AL. 2013. Aberrant functional network recruitment of posterior parietal cortex in Turner syndrome. Hum Brain Mapp 34:3117–3128.

Bruandet M, Molko N, Cohen L, Dehaene S. 2004. A cognitive characterization of dyscalculia in Turner syndrome. Neuropsychologia. 42:288–298.

Buckner RL, Krienen FM, Yeo BT. 2013. Opportunities and limitations of intrinsic functional connectivity MRI. Nat Neurosci. 16:832–837.

Buckner RL, Sepulcre J, Talukdar T, Krienen FM, Liu H, Hedden T, Andrews-Hanna JR, Sperling RA, Johnson KA. 2009. Cortical hubs revealed by intrinsic functional connectivity: mapping, assessment of stability, and relation to Alzheimer's disease. J Neurosci. 29:1860–1873.

Chen ZJ, He Y, Rosa P, Germann J, Evans AC. 2008. Revealing modular architecture of human brain structural networks by using cortical thickness from MRI. Cereb Cortex. 18:2374–2381.

Cox RW. 1996. AFNI: software for analysis and visualization of functional magnetic resonance neuroimages. Comput Biomed Res. 29:162–173.

Cutter WJ, Daly EM, Robertson DM, Chitnis XA, van Amelsvoort TA, Simmons A, Ng VW, Williams BS, Shaw P, Conway GS, et al. 2006. Influence of X chromosome and hormones on human brain development: a magnetic resonance imaging and proton magnetic resonance spectroscopy study of Turner syndrome. Biol Psychiatry. 59:273–283.

Di Martino A, Yan CG, Li Q, Denio E, Castellanos FX, Alaerts K, Anderson JS, Assaf M, Bookheimer SY, Dapretto M, et al. 2014. The autism brain imaging data exchange: towards a large-scale evaluation of the intrinsic brain architecture in autism. Mol Psychiatry. 19:659–667.

Di Martino A, Zuo XN, Kelly C, Grzadzinski R, Mennes M, Schvarcz A, Rodman J, Lord C, Castellanos FX, Milham MP. 2013. Shared and distinct intrinsic functional network centrality in autism and attention-deficit/hyperactivity disorder. Biol Psychiatry. 74:623–632.

Fonov V, Evans AC, Botteron K, Almli CR, McKinstry RC, Collins DL, Brain Development Cooperative G. 2011. Unbiased average age-appropriate atlases for pediatric studies. Neuroimage. 54:313–327.

Fox MD, Snyder AZ, Vincent JL, Corbetta M, Van Essen DC, Raichle ME. 2005. The human brain is intrinsically organized into dynamic, anticorrelated functional networks. Proc Natl Acad Sci U S A. 102:9673–9678.

Friston KJ, Holmes AP, Worsley KJ, Poline JP, Frith CD, Frackowiak RSJ. 1994. Statistical parametric maps in functional imaging: A general linear approach. Hum Brain Mapp. 2:189–210.

Gotts SJ, Simmons WK, Milbury LA, Wallace GL, Cox RW, Martin A. 2012. Fractionation of social brain circuits in autism spectrum disorders. Brain. 135:2711–2725.

Greicius M. 2008. Resting-state functional connectivity in neuropsychiatric disorders. Curr Opin Neurol. 21:424–430.

Greicius MD, Krasnow B, Reiss AL, Menon V. 2003. Functional connectivity in the resting brain: a network analysis of the default mode hypothesis. Proc Natl Acad Sci USA. 100:253–258.

Haberecht MF, Menon V, Warsofsky IS, White CD, Dyer-Friedman J, Glover GH, Neely EK, Reiss AL. 2001. Functional neuroanatomy of visuo-spatial working memory in turner syndrome. Hum Brain Mapp. 14:96–107.

Hampson M, Driesen NR, Skudlarski P, Gore JC, Constable RT. 2006. Brain connectivity related to working memory performance. J Neurosci. 26:13338–13343.

Hart SJ, Davenport ML, Hooper SR, Belger A. 2006. Visuospatial executive function in Turner syndrome: functional MRI and neurocognitive findings. Brain. 129:1125–1136.

He Y, Wang JH, Wang L, Chen ZJ, Yan CG, Yang H, Tang HH, Zhu CZ, Gong QY, Zang YF, et al. 2009. Uncovering intrinsic modular organization of spontaneous brain activity in humans. PLoS One. 4:e5226.

Holzapfel M, Barnea-Goraly N, Eckert MA, Kesler SR, Reiss AL. 2006. Selective alterations of white matter associated with visuospatial and sensorimotor dysfunction in turner syndrome. J Neurosci. 26:7007–7013.

Hong DS, Bray S, Haas BW, Hoeft F, Reiss AL. 2014. Aberrant neurocognitive processing of fear in young girls with Turner syndrome. Soc Cogn Affect Neurosci. 9:255–264.

Hong DS, Hoeft F, Marzelli MJ, Lepage JF, Roeltgen D, Ross J, Reiss AL. 2014. Influence of the X-chromosome on neuroanatomy: evidence from Turner and Klinefelter syndromes. J Neurosci. 34:3509–3516.

Hong DS, Reiss AL. 2012. Cognition and behavior in Turner syndrome: a brief review. Pediatr Endocrinol Rev: PER. 9:710–712.

Johnson W, Carothers A, Deary IJ. 2009. A role for the X chromosome in sex differences in variability in general intelligence? Perspect Psychol Sci. 4:598–611.

Kennedy DP, Adolphs R. 2012. The social brain in psychiatric and neurological disorders. Trends Cogn Sci. 16:559–572.

Kesler SR, Haberecht MF, Menon V, Warsofsky IS, Dyer-Friedman J, Neely EK, Reiss AL. 2004. Functional neuroanatomy of spatial orientation processing in Turner syndrome. Cereb Cortex. 14:174–180.

Kesler SR, Menon V, Reiss AL. 2006. Neuro-functional differences associated with arithmetic processing in Turner syndrome. Cereb Cortex. 16:849–856.

Kotter R, Stephan KE. 2003. Network participation indices: characterizing component roles for information processing in neural networks. Neural Netw. 16:1261–1275.

Lehrke R. 1972. A theory of X-linkage of major intellectual traits. Am J Ment Defic. 76:611–619.

Lepage JF, Clouchoux C, Lassonde M, Evans AC, Deal CL, Theoret H. 2013. Abnormal motor cortex excitability is associated with reduced cortical thickness in X monosomy. Hum Brain Mapp. 34:936–944.

Lepage JF, Hong DS, Mazaika PK, Raman M, Sheau K, Marzelli MJ, Hallmayer J, Reiss AL. 2013. Genomic imprinting effects of the X chromosome on brain morphology. J Neurosci. 33:8567–8574.

Lepage JF, Mazaika PK, Hong DS, Raman M, Reiss AL. 2013. Cortical brain morphology in young, estrogen-naive, and adolescent, estrogen-treated girls with Turner syndrome. Cereb Cortex. 23:2159–2168.

Liang X, Zou Q, He Y, Yang Y. 2013. Coupling of functional connectivity and regional cerebral blood flow reveals a physiological basis for network hubs of the human brain. Proc Natl Acad Sci USA. 110:1929–1934.

Marzelli MJ, Hoeft F, Hong DS, Reiss AL. 2011. Neuroanatomical spatial patterns in Turner syndrome. Neuroimage. 55:439–447.

Mazzocco MM. 2006. The cognitive phenotype of Turner syndrome: specific learning disabilities. Int Congr Ser. 1298:83–92.

Molko N, Cachia A, Riviere D, Mangin JF, Bruandet M, LeBihan D, Cohen L, Dehaene S. 2004. Brain anatomy in Turner syndrome: evidence for impaired social and spatial-numerical networks. Cereb Cortex. 14:840–850.

Molko N, Cachia A, Rivière D, Mangin J-F, Bruandet M, Le Bihan D, Cohen L, Dehaene S. 2003. Functional and structural alterations of the intraparietal sulcus in a developmental dyscalculia of genetic origin. Neuron. 40:847–858.

Mullaney R, Murphy D. 2009. Turner syndrome: neuroimaging findings: structural and functional. Dev Disabil Res Rev. 15:279–283.

Murphy DGM, Decarli C, Daly E, Haxby JV, Allen G, White BJ, Mcintosh AR, Powell CM, Horwitz B, Rapoport SI, et al. 1993. X-Chromosome effects on female brain - a magnetic-resonance-imaging study of Turners-syndrome. Lancet. 342:1197–1200.

Newman ME. 2006. Modularity and community structure in networks. Proc Natl Acad Sci USA. 103:8577–8582.

Power JD, Barnes KA, Snyder AZ, Schlaggar BL, Petersen SE. 2012. Spurious but systematic correlations in functional connectivity MRI networks arise from subject motion. Neuroimage. 59:2142–2154.

Raichle ME. 2010. Two views of brain function. Trends Cogn Sci. 14:180–190.

Raznahan A, Cutter W, Lalonde F, Robertson D, Daly E, Conway GS, Skuse DH, Ross J, Lerch JP, Giedd JN, et al. 2010. Cortical anatomy in human X monosomy. Neuroimage. 49:2915–2923.

Raznahan A, Probst F, Palmert MR, Giedd JN, Lerch JP. 2013. High resolution whole brain imaging of anatomical variation in XO, XX, and XY mice. Neuroimage. 83:962–968.

Reiss AL, Mazzocco MMM, Greenlaw R, Freund LS, Ross JL. 1995. Neurodevelopmental effects of X monosomy: a volumetric imaging study. Ann Neurol. 38:731–738.

Ropers HH, Hamel BC. 2005. X-linked mental retardation. Nat Rev Genet. 6:46–57.

Rovet J. 2004. Turner syndrome: a review of genetic and hormonal influences on neuropsychological functioning. Child Neuropsychol. 10:262–279.

Skuse DH. 2005. X-linked genes and mental functioning. Hum Mol Genet. 14:R27–R32.

Sowell ER, Peterson BS, Kan E, Woods RP, Yoshii J, Bansal R, Xu DR, Zhu HT, Thompson PM, Toga AW. 2007. Sex differences in cortical thickness mapped in 176 healthy individuals between 7 and 87 years of age. Cereb Cortex. 17:1550–1560.

Sporns O, Chialvo DR, Kaiser M, Hilgetag CC. 2004. Organization, development and function of complex brain networks. Trends Cogn Sci. 8:418–425.

Sporns O, Tononi G, Edelman GM. 2000. Theoretical neuroanatomy: relating anatomical and functional connectivity in graphs and cortical connection matrices. Cereb Cortex. 10:127–141.

Sybert VP, McCauley E. 2004. Turner's syndrome. N Engl J Med. 351:1227–1238.

Tamm L, Menon V, Reiss AL. 2003. Abnormal prefrontal cortex function during response inhibition in turner syndrome: functional magnetic resonance imaging evidence. Biol Psychiatry. 53:107–111.

Tomasi D, Volkow ND. 2010. Functional connectivity density mapping. Proc Natl Acad Sci USA. 107:9885–9890.

Turner G. 1996. Intelligence and the X chromosome. Lancet. 347:1814–1815.

Wang L, Dai Z, Peng H, Tan L, Ding Y, He Z, Zhang Y, Xia M, Li Z, Li W, et al. 2014. Overlapping and segregated resting-state functional connectivity in patients with major depressive disorder with and without childhood neglect. Hum Brain Mapp. 35:1154–1166.

Wei T, Liang X, He Y, Zang Y, Han Z, Caramazza A, Bi Y. 2012. Predicting conceptual processing capacity from spontaneous neuronal activity of the left middle temporal gyrus. J Neurosci. 32:481–489.

Wei W, Chen C, Yang T, Zhang H, Zhou X. 2014. Dissociated neural correlates of quantity processing of quantifiers, numbers, and numerosities. Hum Brain Mapp. 35:444–454.

Wei W, Lu H, Zhao H, Chen C, Dong Q, Zhou X. 2012. Gender differences in children's arithmetic performance are accounted for by gender differences in language abilities. Psychol Sci. 23:320–330.

Xia M, Wang J, He Y. 2013. BrainNet Viewer: a network visualization tool for human brain connectomics. PLoS One. 8: e68910.

Xie S, Zhang Z, Zhao Q, Zhang J, Zhong S, Bi Y, He Y, Pan H, Gong G. 2015. The effects of X chromosome loss on neuroanatomical and cognitive phenotypes during adolescence: a multimodal structural MRI and diffusion tensor imaging study. Cereb Cortex. 25:2842–2853.

Yamagata B, Barnea-Goraly N, Marzelli MJ, Park Y, Hong DS, Mimura M, Reiss AL. 2012. White matter aberrations in prepubertal estrogen-naive girls with monosomic Turner syndrome. Cereb Cortex. 22:2761–2768.

Yan C-G, Zang Y-F. 2010. DPARSF: A MATLAB Toolbox for "Pipeline" Data Analysis of Resting-State fMRI. Front Syst Neurosci. 4:13.